University of Stavanger

FACULTY OF SCIENCE AND TECHNOLOGY

MASTER'S THESIS

Study programme/specialisation: Engineering Structures and Materials/ Mechanical Systems	Spring semester, 2020 Open
Author: Erik Årdal Zürcher	
Programme coordinator: Dimitrios Pavlou Supervisor(s): Dimitrios Pavlou	
Title of master's thesis: **Cost Improvement of Seal Retainer**	
Credits: 30	
Keywords: Subsea, tool design, reducing costs, seal retainer, optimization	Number of pages: 40 + Appendix: 2 pages Stavanger, 01/06/2020

Title page for master's thesis
Faculty of Science and Technology

Summary

The objectives of the thesis are to optimize the tip angle of the seal retainers and to determine cheaper materials that are appropriate for the application of the tool. Seal retainers are used to retain seals on valve blocks in subsea environments. The functionality of the tool must be maintained, while the tool must be optimized based on performance and costs.

Firstly, the thesis includes analysis of stresses to ensure sufficient strength of the tool. The major stresses in the seal retainer for various tip angles are evaluated. Both the analytical and numerical results agree. The 40° tip angle is found to be superior. The proposed 40° tip angle leads to a line contact between the retainer and the seal resulting in far lower contact stresses compared to point contacts. The determined stress results also inform about the necessary strength for the seal retainer. The required yield strength is determined to be unnecessarily high with the current tip angle of 45°. If the tip angle is changed to the superior tip angle of 40°, the strength requirement will be substantially lowered. In that case, the bending stress will be the limiting factor. The strength requirement of the retainer's material can potentially be lowered further by increasing the diameter of the pin. However, that will result in a costly initial investment.

Secondly, relatively many steel grades with martensitic structure from various treatments can achieve high strengths. However, the material of the retainer must also have sufficient corrosion resistance in the subsea environment. Hence, stainless steel is identified to be the only type of steel that can meet the corrosion resistance requirement. In addition, the current protective coating must be continued in being used for the retainer. With all the requirements considered, a list of the most appropriate stainless steels is presented. The list is obtained from evaluating the alloy surcharges of commercially available stainless steel grades over a one year period. The list is also based on the yield strengths of each stainless steel grade with various strength increasing treatments. The winner of the analysis is the stainless steel grade EN 1.4034.

Preface

The thesis marks the end of the master's degree in Engineering Structures and Materials with a specialization in Mechanical Systems at the University of Stavanger (UiS). The thesis was written in cooperation with Aker Solutions Tranby and UiS.

I would like to thank my supervisor Dimitrios Pavlou from UiS for guiding me during the thesis. He is both knowledgeable and structured, which proved to be invaluable during the semester. I would also like to thank the other professors and staff from UiS for teaching and guidance during the master's degree.

I would like to thank A. Bakken, D. Skogen, and O. Torvanger from Aker Solutions Tranby. My appreciation goes to A. Bakken for being a great supervisor during the thesis and the summer internship in 2019. My gratitude goes to D. Skogen for identifying the thesis topic, and O. Torvanger for giving me the opportunity to write the thesis.

I would also like to thank my family and classmates for supporting me and sharing knowledge during the master's degree.

Table of Contents

List of Tables

List of Figures

Nomenclature

Symbol	Description	Unit
d	Diameter	m
Y	Yield strength / 0.2% proof stress	Nm^{-2}
τ_{max}	Maximum shear stress	Nm^{-2}
A_c	Constant related to geometry and configuration of the two bodies in contact	m^{-1}
B_c	Constant related to geometry and configuration of the two bodies in contact	m^{-1}
R_1, R_1'	Radii of contact body 1	m
R_2, R_2'	Radii of contact body 2	m
W	Section modulus	m^3
I	Second moment of area	m^4
M_b	Bending moment	Nm
$M_{b,max}$	Maximum bending moment	Nm
σ_b	Bending stress	Nm^{-2}
$\sigma_{b,max}$	Maximum bending stress	Nm^{-2}
σ_{max}	Maximum stress / maximum principal stress	Nm^{-2}
α	Angle between principal planes of curvature	$^\circ$
E	Modulus of elasticity	Nm^{-2}
v	Poisson's ratio	-
$\sigma_{oct,max}$	Maximum octahedral stress	Nm^{-2}
c_{sigma}	Coefficient used for contact stress applications	-
c_{tau}	Coefficient used for contact stress applications	-
c_G	Coefficient used for contact stress applications	-
c_b	Coefficient used for contact stress applications	-
b	Semiminor axis of the area of contact	m
Δ	Value used for determining contact stresses	m^3N^{-1}
P	Force exerted by one body on the other body	N
w	Load distribution over a distance	Nm^{-1}
L	Length	m
P_{cr}	Critical buckling force	N
F_{cr}	Critical axial force	N
F_s	Force exerted by the spring	N
R	Reaction force from the seal when in contact with the pin	N
$F_{n,max}$	Maximum normal force	N
$\sigma_{n,max}$	Maximum normal stress	Nm^{-2}
A	Area	m^2

Abbreviations

MVB	=	Master Valve Block
Pin	=	Seal Retainer Pin
Retainer	=	Seal Retainer
Seal	=	Seal on the Master Valve Block
TTT Diagram	=	Time-Temperature-Transformation Diagram
UiS	=	University of Stavanger

Chapter 1

Introduction

The extraction of oil resources offshore requires complex and robust equipment and tools. The subsurface environment offshore is called subsea. Subsea environments present challenges for engineers as one must overcome obstacles e.g. high pressure and corrosion due to seawater. The subsea designs must be reliable, robust, and cost-competitive while performing demanding tasks. Aker Solutions have many great engineers facing the demanding tasks and being competitive while doing so.

The objectives of the thesis are to optimize the tip angle of the seal retainers and to determine cheaper materials that are appropriate for the application of the tool. Seal retainers are used to retain seals on valve blocks in subsea environments. A total of four retainers are used for each seal. The functionality of the tool must be maintained, while the tool must be optimized based on performance and costs.

The Aker Solutions Tranby department have a workshop where they produce a great variety of complex products. The production system has a large variety of tasks e.g. designing, machine programming, planning, administration, etc. Changes in the design will affect many of the other tasks. There will always be initial costs related to designs being adjusted or changed. The same applies to even the most minor adjustments imaginable.

This is why the flexibility for change in the production system must be considered a constraining factor. The interface toward the master valve block is e.g. difficult to change at this moment in time as it results in an initial high cost investment. Hence, as long as solutions work efficiently and to the satisfaction of customers, engineers must preserve these solutions. However, there are always possibilities of changing or adjusting certain features of tools. The material of the seal retainer and the tip angle of the pin can be changed without a large financial investment.

The thesis includes analysis of stresses to ensure sufficient strength of the tool. The major stresses in the seal retainer for various tip angles are evaluated. The contact stresses between the seal and the pin are evaluated both analytically and numerically. The numerical results are obtained by ANSYS simulations. Both the analytical and numerical results agree. The 40° tip angle is found to be superior. The 40° tip angle leads to a line contact

between the retainer and the seal resulting in far lower contact stresses compared to the current tip angle of 45°, and other possible tip angles. The determined stress results also inform about the necessary strength for the seal retainer. The required yield strength is determined to be unnecessarily high with the current tip angle. If the tip angle is changed to the superior tip angle of 40°, the strength requirement will be substantially lowered. In that case, the bending stress will be the limiting factor. The strength requirement of the retainer's material can potentially be lowered further by increasing the diameter of the pin. However, that will result in a costly initial investment.

Relatively many steel grades with martensitic structure from various treatments can achieve high strengths. However, the material of the retainer must also have sufficient corrosion resistance in the subsea environment. Hence, stainless steel is identified to be the only type of steel that can meet the corrosion resistance requirement. In addition, the current protective coating must be continued in being used for the retainer. With all the requirements considered, a list of the most appropriate stainless steels is presented. The list is obtained from evaluating the alloy surcharges of commercially available stainless steel grades over a one year period. The list is also based on the yield strengths of each stainless steel grade with various strength increasing treatments. The winner of the analysis is the stainless steel grade EN 1.4034.

The following paragraphs present the layout of the report. The following chapters include theory, analysis, results, discussion, and conclusion.

In chapter 2, the theory will be covered. The chapter is divided into three sections. The first section is about Tresca's and von Mieses's yield criterion for shear stress. The second section is about the theory of contact stresses. The third section is about bending, buckling, and axial loading.

In chapter 3, the analysis will be covered. The chapter explains the methods and the assumptions that led to the results. The first two sections are about the material selection of the seal retainer. The next section is about the methods and the assumptions for the analytical and the numerical calculations of the contact stresses. The last section in chapter 3 shows the free-body diagrams used to determine the stresses and the critical forces.

Chapter 4 covers all the determined results. The first section shows the ranking of stainless steels. The second section covers the analytical and numerical results of contact stresses with different tip angles. The next two sections cover the remaining results. The last chapter compares all the results with the requirements to gain acceptance of the tool.

Chapter 5 discusses the functionalities, geometries, and materials of each component of the seal retainer and the seal. The chapter also compares the current material of the seal retainer with the proposed material. There are discussions about material treatments, structures, and the effects of alloying elements. The chapter also discusses the numerical results with pictures of the results from the software.

In chapter 6, the conclusions of the thesis will be stated. The first section is about material selection. The second section is about the superior tip angle for the pin of the seal retainer. The chapter includes the advantages and disadvantages of the proposed material and tip angle. The last section of the chapter includes further research suggestions.

The appendix shows the technical assembly drawing of the redesigned seal retainer.

Chapter 2

Basic Theory

2.1 Yielding of Materials

Tresca and von Mieses are generally used to compare the maximum shear stresses against the required yield strength of a material. Tresca is a slightly more conservative requirement compared to von Mieses. A more conservative requirement results in a higher degree of safety. Hence, the safe choice is to use Tresca's criterion. Thus, Tresca's criterion for yielding was used in the thesis.

Tresca criterion for yielding under pure shear stress [7]:

$$\tau_{max} = \frac{Y}{2} = 0.5Y \tag{2.1}$$

Where: Y = yield strength
τ_{max} = maximum shear stress

Von Mieses criterion for yielding under pure shear stress [7]:

$$\tau_{max} = \frac{Y}{\sqrt{3}} \approx 0.577Y \tag{2.2}$$

Comparison between Tresca- and von Mieses criterion according to Boresi and Schmidt in the sixth edition of Advanced Mechanics of Materials argue the following [7]. The Tresca criterion is a more conservative estimate of the yield [7]. The yield shear stress τ_Y for some ductile metals has been experimentally found to be approximately 15% higher than the Tresca predicted value [7].

2.2 Contact Stresses

The following formulas and diagrams can be used to determine the contact stresses. It is important to determine the contact stresses to gain knowledge about the required strength

of a material. For example, when there are combinations of high forces and sharp curvatures in the contact zone, the stresses can be very high. The higher the contact stresses are, the higher the strength of the materials will have to be. The combination of low strength materials and high contact stresses can lead to yielding or failures. Yielding is when the deformations are non-reversible.

Determining the constants B_c and A_c according to Boresi and Schmidt [7]:

Determining B_c [7]:

$$B_c = \frac{1}{4}\left(\frac{1}{R_1} + \frac{1}{R_2} + \frac{1}{R_1'} + \frac{1}{R_2'}\right) + \frac{1}{4}\sqrt{\left[\left(\frac{1}{R_1} - \frac{1}{R_1'}\right) + \left(\frac{1}{R_2} - \frac{1}{R_2'}\right)\right]^2 - 4\left(\frac{1}{R_1} - \frac{1}{R_1'}\right)\left(\frac{1}{R_2} - \frac{1}{R_2'}\right)\sin^2\alpha} \quad (2.3)$$

Where $R_1, R_1', R_2, \; and \; R_2'$ are the four radii of the two bodies in contact [7]. α is the angle between the corresponding planes of the principal curvatures [7].

Determining A_c [7]:

$$A_c = \frac{1}{4}\left(\frac{1}{R_1} + \frac{1}{R_2} + \frac{1}{R_1'} + \frac{1}{R_2'}\right) - \frac{1}{4}\sqrt{\left[\left(\frac{1}{R_1} - \frac{1}{R_1'}\right) + \left(\frac{1}{R_2} - \frac{1}{R_2'}\right)\right]^2 - 4\left(\frac{1}{R_1} - \frac{1}{R_1'}\right)\left(\frac{1}{R_2} - \frac{1}{R_2'}\right)\sin^2\alpha} \quad (2.4)$$

Where $R_1, R_1', R_2, \; and \; R_2'$ are the four radii of the two bodies in contact [7]. α is the angle between the corresponding planes of the principal curvatures [7].

The contact stresses and coefficients are determined by the following equations according to Boresi and Schmidt [7]:

$$\sigma_{max} = -c_\sigma \frac{b}{\Delta} \quad (2.5)$$

$$\tau_{max} = c_\tau \frac{b}{\Delta} \quad (2.6)$$

$$\tau_{oct,max} = c_G \frac{b}{\Delta} \quad (2.7)$$

Where [7]:

$$\Delta = \frac{2(1 - v^2)}{(A + B)E} \quad (2.8)$$

For a point contact [7]:

$$b = c_b(P\Delta)^{\frac{1}{3}} \tag{2.9}$$

For a line contact [7]:

$$b = \sqrt{\frac{2w\Delta}{\pi}} \tag{2.10}$$

Where w is the load per unit length of the line contact [7].

The coefficients c_σ, c_τ, c_G, and c_b can be determined using the diagrams shown in Fig. 2.1 and Fig. 2.2 with values of B_c/A_c [7]. For a line contact, the ratio B_c/A_c is ∞ [7]. However, the values of the coefficients c_σ, c_τ, c_G are constant over B_c/A_c ratios approximately equal to 50 [7].

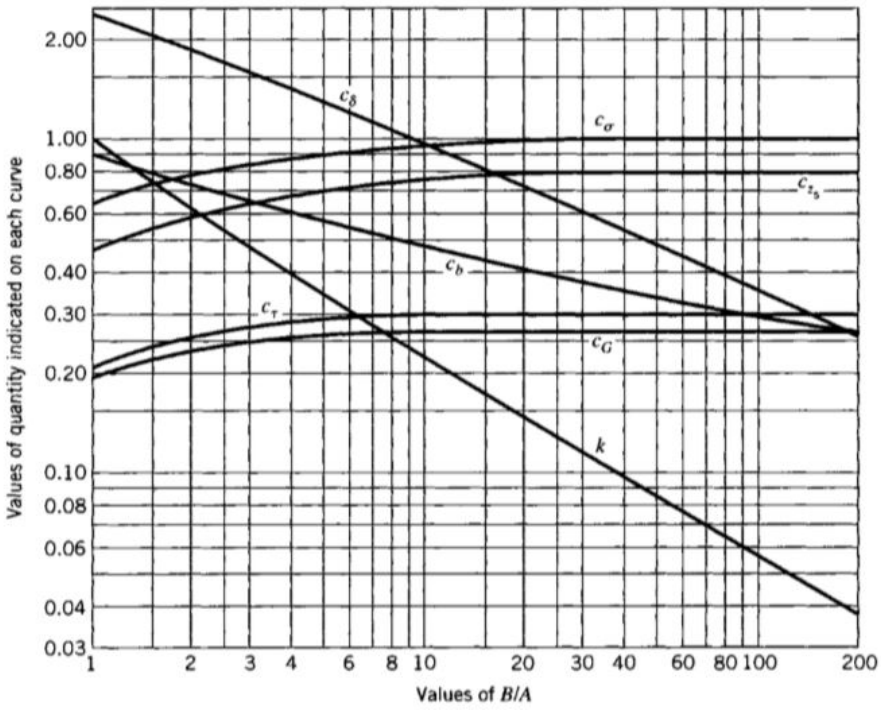

Figure 2.1: Stress and deflection coefficients for two bodies at a point contact [7].

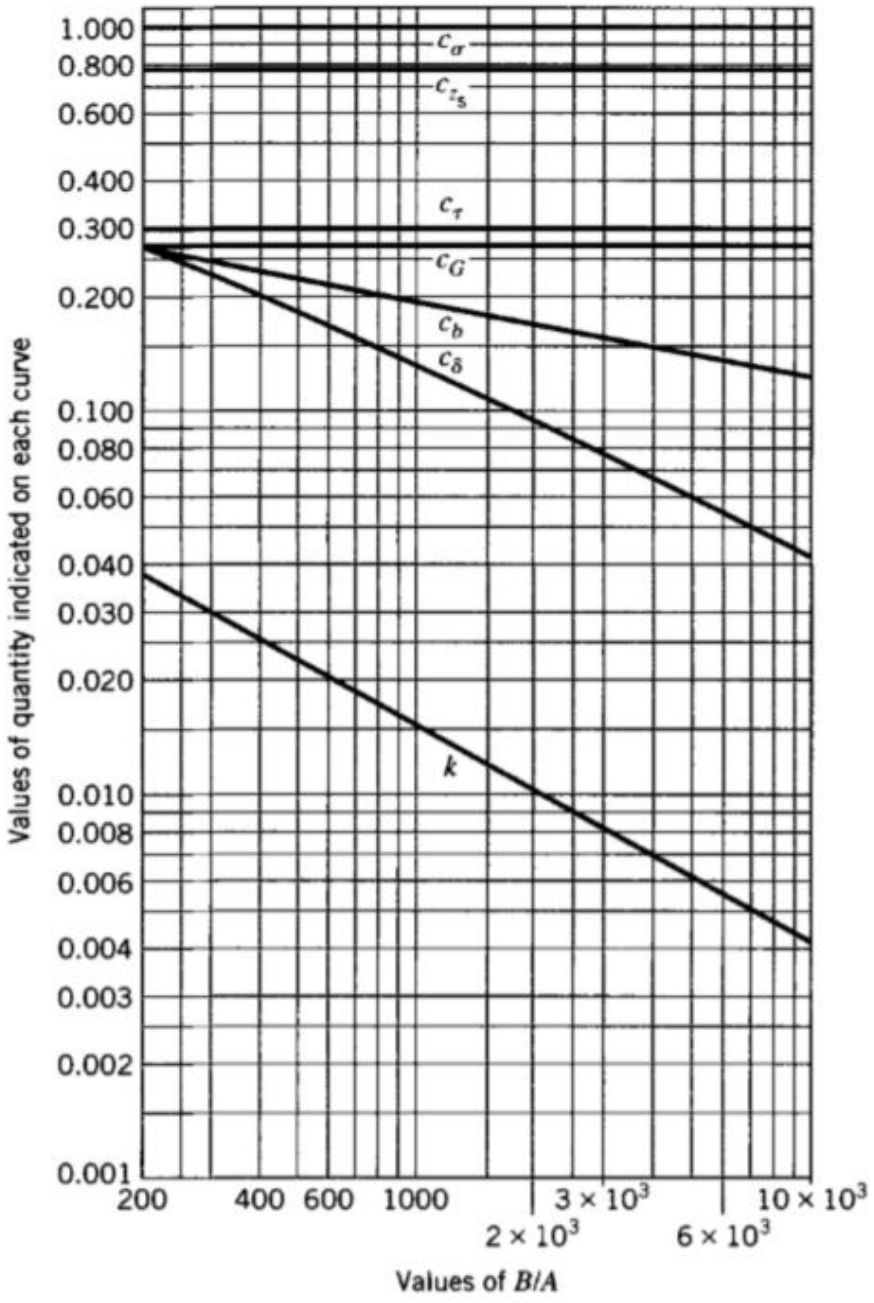

Figure 2.2: Stress and deflection coefficients for two bodies at a point contact [7].

2.3 Bending, Buckling and Axial Loading

The following formulas are used to determine the maximum normal stress, the critical buckling force, the critical axial force, and the maximum bending stress. The results from the formulas are used to determine the required strength of the material. Higher stresses result in need of a higher strength material. Higher critical forces compared to the loads result in a lower requirement of strength. If any of the stresses are higher than the yield

strength, non-reversible deformations or failures will occur. If any critical forces are lower than the loads, non-reversible deformations or failures will occur. Hence, it is important to determine the stresses and critical forces.

The following equations are according to Boresi and Schmidt [7].

Maximum normal stress in a pin [7]:

$$\sigma_{n,max} = \frac{F_{n,max}}{A} \tag{2.11}$$

Where [7]:

$$A = \frac{\pi}{4} d^2 \tag{2.12}$$

Critical buckling force for a pin [7]:

$$P_{cr} = \frac{EI\pi^2}{L^2} \tag{2.13}$$

Where [7]:

$$I = \frac{\pi d^4}{64} \tag{2.14}$$

Critical axial force in a pin [7]:

$$\sigma_{cr} = Y = \frac{F_{cr}}{A} \tag{2.15}$$

Where [7]:

$$A = \frac{\pi}{4} d^2 \tag{2.16}$$

Maximum bending stress in a pin [7]:

$$\sigma_{b,max} = \frac{M_{b,max}}{W} \tag{2.17}$$

Where [7]:

$$W = \frac{\pi d^3}{32} \tag{2.18}$$

Chapter 3

Analysis

3.1 Material of the Seal Retainer

The material of the seal retainer needs to possess a certain amount of corrosion resistance in the subsea saltwater environment. A popular choice in subsea environments is the use of sacrificial anodes for corrosion protection. However, the housing is resting on the o-rings of the pin, which are of a polymer. Hence, there would most likely not be electrical conductivity as the polymer o-rings are non-magnetic. The assumption must be tested in an experiment in order to be verified. Hence, the coating that is being used today should be continued in being used. In addition, the material of the retainer must be of stainless steel to have sufficient corrosion resistance.

3.2 Stainless Steel Pricing

The calculation of stainless steel prices are generally divided into three parts. The three parts are the base price, the alloy surcharge and the extras [8].

The aim of the base price is to cover the stainless steel suppliers labour costs, machinery costs, maintenance costs, administration costs, etc, and will also follow market trends [8]. The base cost will be different for each supplier. This is because of reasons such as regional variations in salaries and whether a supplier prioritises quantity or quality. Some suppliers also require customers to buy a certain minimum amount of steel, and the base price will be affected by the customers' order size.

The aim of the alloy surcharge is to price stainless steels based on the price of their alloying elements. Higher amounts of expensive alloys will increase the alloy surcharge. Alloys such as nickel, chromium and molybdenum are very expensive, and therefore steels with high amounts of these will have a higher alloy surcharge [8]. The price of alloy ores experiences daily fluctuations, and therefore the alloy surcharge will also fluctuate. The stainless steel suppliers expect customers to pay for the necessary alloys, and that is why

the alloy surcharge is utilized [8]. The alloy surcharge is, thus, often what makes some steels much more expensive compared to others.

The extra cost is based on the customers' needs within packaging, delivery time, dimensions, etc [8].

The aim of the material selection is to help Aker Solutions in determining a cheaper stainless steel for the retainer. Hence, the alloy surcharge is an important factor in buying cheaper steels. The material which is currently used has an expensive chemical composition. Inconel 718 has 50–55% nickel [9], which is one of the most expensive alloying elements used in stainless steels. Thus, finding a stainless steel with lower amounts of expensive alloys will greatly contribute in lowering the material price. The new stainless steel will need the cheapest combination of alloys while maintaining a satisfactory yield strength.

The mean of the monthly alloy surcharges for stainless steels between March 2019 and March 2020 is used during the analysis. The alloy surcharges data for each month were gathered from the Finish global stainless steel company Outokumpu [1]. The alloy surcharges for the European continent were used. The steels were then sorted based on the mean alloy surcharges over the one year period. The mechanical properties of all the steels and with all treatments were then analyzed. This required evaluations of several hundred sources. The stainless steels were then ranked based on the mean alloy surcharges divided by the yield strengths. Equation 3.1 shows the formula that was used to evaluate each steel. The steel with the lowest number from Eq. 3.1 would be awarded with the best ranking. This is due to the fact that lower numbers from Eq. 3.1 would be a consequence of lower costs of steel and higher yield strengths.

$$Number\ used\ for\ ranking = \frac{Mean\ alloy\ surcharges\ [kr/ton]}{Yield\ strength\ [MPa]} \tag{3.1}$$

The method of alloy surcharges was cross-checked and validated using a list of total steel prices determined by web searches, emails, phone calls, etc. Both methods matched, which validated the alloy surcharges approach. As expected, lower costs on alloy surcharges would result in lower total steel prices. The method of alloy surcharges was therefore used in the thesis.

3.3 Tip Angle Optimization

The tip angle is 45° and the assembly angle is 50° to the horizontal plane today. This means that the edge of the pin tip is currently in contact with the seal. The edge of the pin has a low radii geometry and may cause damage to the seal. A tip angle of 40° would result in a line contact at the pin face between the edge and the tip. Tip angles below 40° would result in tip contact with the seal. This is directly due to the 50° stationary installation angle.

The analytical hand calculations were carried out assuming smooth contact (no friction) between the pin and the seal. Smooth contact could be assumed because both the

pin and the seal would be stationary. The temperature variations were neglected in the analytical analysis but included in the numerical analysis.

In the following three paragraphs, the assumptions for the analytical contact stress calculations are stated for each case. The difference between each case was the tip angle of the pin. The different tip angles resulted in different geometries of the pin near the contact zone.

In case 1, the pin's contact area was toroid-shaped and the seal was cylinder-shaped. The two contact surfaces were in point contact. Case 1a would use the maximum allowable edge radius after machining of 0.6 mm according to the machine drawing. Case 1b would use half of the maximum allowable radius equalling 0.3 mm. The maximum allowable edge radius was used in all the cases except case 1b in the analytical calculation.

In case 2, the pin's contact geometry would, in reality, be a cone-shaped. However, this geometry was simplified to be a cylinder with the radius equal to the average between the maximum and minimum of the cone radius. This simplification was only used for the analytical analysis. For the numerical analysis, the exact geometry was used. The two contact surfaces would be in line contact for case 2.

In case 3, the pin's contact geometry was slightly simplified to be a sphere. The two contact surfaces would be in a point contact. Figure 3.1 shows the seal with its contact zone in the middle.

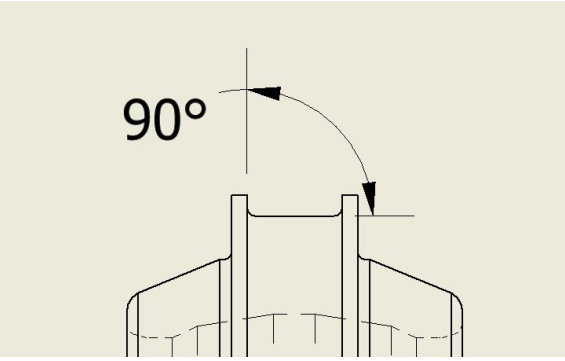

Figure 3.1: The contact angle of the seal.

For the numerical analysis, ANSYS Workbench was used. All the numerical results were obtained by using ANSYS's software [10]. Both the retainer and seal were simplified so that all geometry near the contact area would be included, and all the unnecessary material was removed. The remaining geometry for the seal is shown in Fig. 3.2. All the computational drawings were designed with the aid of using Autodesk's Inventor software [11].

Three different retainer pins with tip angles of 45°, 40°, and 35° were used for case 1, case 2, and case 3 respectively. The maximum allowable edge radius of 0.6 mm was used for all cases in the numerical analysis. Figure 3.3 shows the simplified geometry of the retainers. The geometry far away from the contact zone was removed because it would not have any effect on the numerical analysis results. Unnecessary material would only

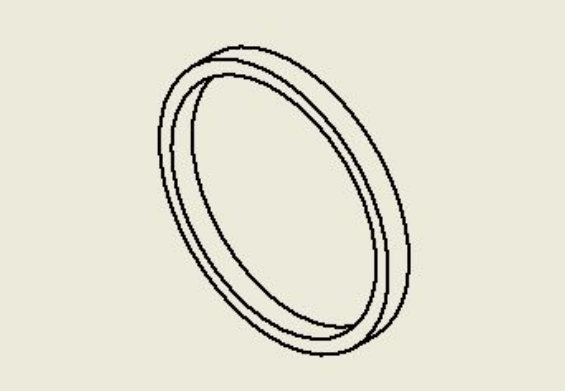

Figure 3.2: Simplification of the seal for the numerical analysis.

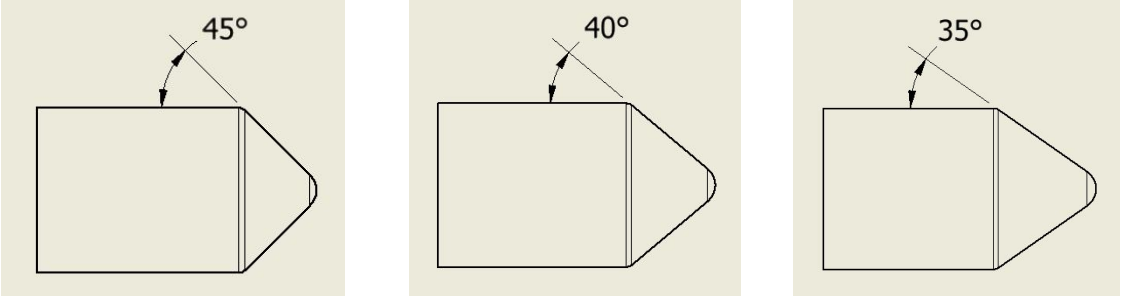

(a) Case 1 **(b)** Case 2 **(c)** Case 3

Figure 3.3: Simulation geometry of retainers for case 1, 2 and 3.

increase the amounts of elements and nodes, which would also increase the running times of the simulations.

The material properties used were of standard steel. This could be done because there are only minor variations in the elasticity modulus and Poisson's ratio between different steel alloys. The seal contacted the pin's edge in case 1, the pin's cone face in case 2, and the pin's tip in case 3. A fine mesh was applied to the contact area of the pin. The pin's mesh would be different for each case depending on where the contact was. A fixed support was used for the inside of the seal. Both axial force and vertical force was simulated. The axial force would be the most realistic scenario, as the spring would push the pin in the axial direction. Hence, the axial force was the most simulated. The vertical force was used in order to compare against the analytical solutions. The pin was constrained against movement in the x- and z-direction. Thermal condition of constant 2 °C was analysed in order to simulate the minimum temperature. Thermal condition of constant 149 °C was analysed in order to simulate the maximum temperature.

The amount of nodes was 982 856 for case 1, 776 693 for case 2 and 706 267 for case 3. Figure 3.4 illustrates the meshing of the seal. The mesh of the seal was the same in all three cases. Figure 3.4a is from a cross-section of the seal, and shows that the size of elements decreased toward the contact surface at the top. Figure 3.4b is taken directly above the contact surface, and it also shows the refinement toward the contact surface. Figure 3.4c

shows the the tetrahedron-shaped mesh at the contact surface in close view. Tetrahedron elements were able to accurately represent the curvatures. Some of the elements away from the contact surface was slightly misshapen by distortions. However, elements close to the contact surface had more optimal shapes. Both the size and the shape of the elements affects the accuracy of the results. The combination of smaller elements and more optimal shaped elements gives the most accurate results.

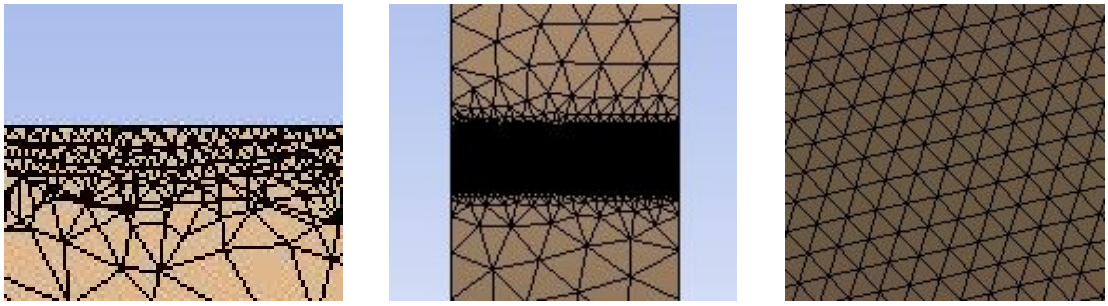

(a) Cross-section **(b)** Above **(c)** Close view above

Figure 3.4: Meshing of the seal.

Figure 3.5 shows the meshing of the pins for the various cases. Figure 3.5a shows the mesh of the pin for case 1. Figure 3.5b shows the mesh of the pin for case 2. Figure 3.5c shows the mesh of the pin for case 3. The mesh is coarse away from the contact area. The mesh transitions toward the contact area, and is highly refined at the contact area. The refinement of the meshes is important because finer meshes will result in more accurate results during numerical analysis. However, if the meshes consist of very small elements throughout the entire geometries, the running times for the simulations will last too long.

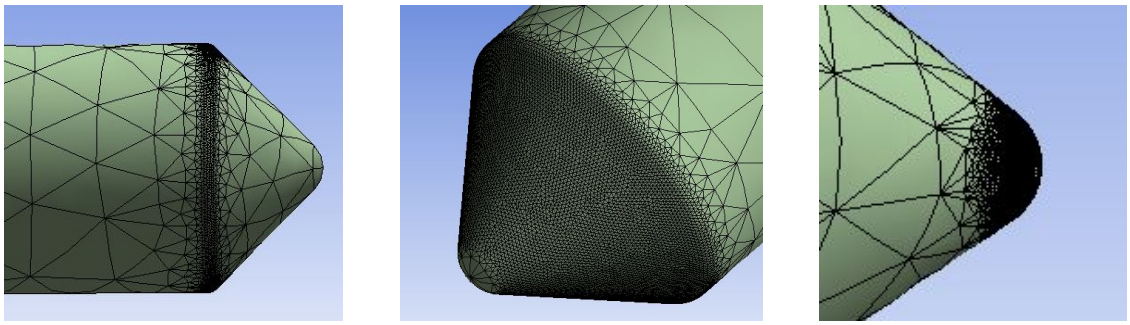

(a) Case 1 **(b)** Case 2 **(c)** Case 3

Figure 3.5: Simulation mesh of retainers for case 1, 2 and 3.

Two different cross-sections were used to analyse the numerical results. The cross-sections were called 'section 1' and 'section 2'. Figure 3.6 shows 'section 1' to the left and 'section 2' to the right.

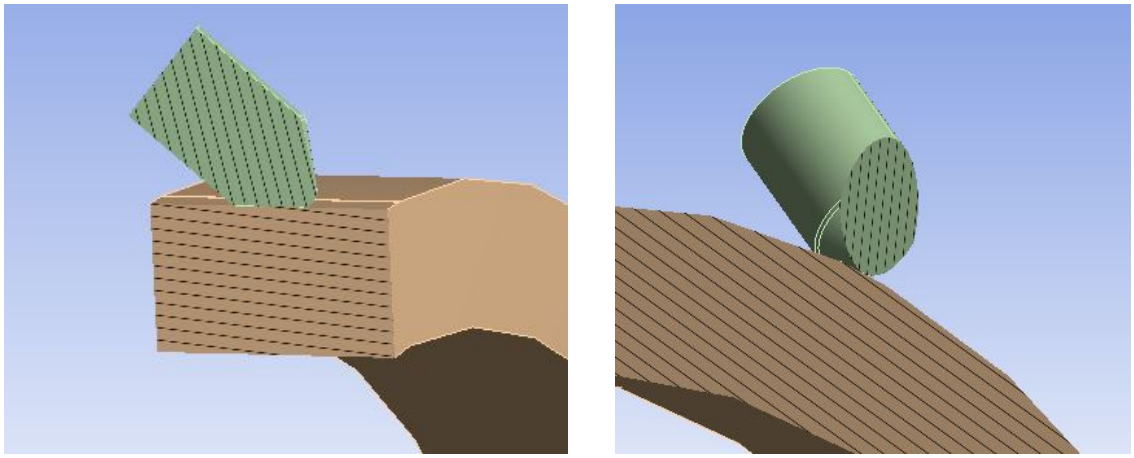

(a) 'Section 1' **(b)** 'Section 2'

Figure 3.6: Explanation of the two different cross-sections used to interpret the results.

3.4 Free-Body Diagrams

Figure 3.7 shows the free-body diagram of the pin when the tip angle is 45°. F_s is the force from the spring which pushes the pin toward the seal. R is the resulting contact force from the seal. A is the simple support from the housing, while w is the triangularly distributed load from the housing. The force R can be decomposed into its horizontal and vertical components. The free-body diagram was utilized to determine the stresses and critical forces. The design pressure was used in every analysis, which led to additional safety margins. The operational pressure was about one third lower than the design pressure.

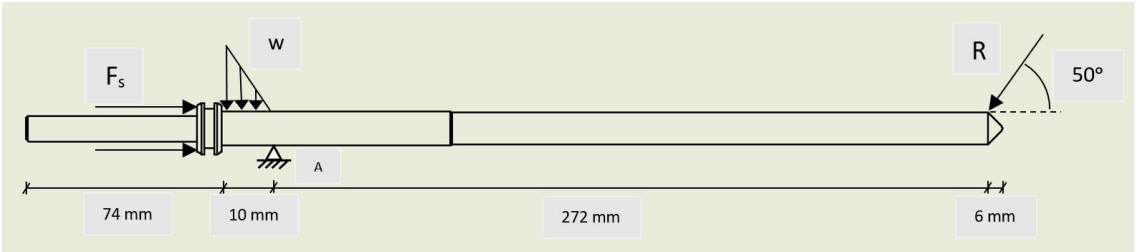

Figure 3.7: Free-body diagram of the pin when the tip angle is 45°.

Figure 3.8 shows the free-body diagram of the pin when the tip angle is 40°. The force R is now located at the cone-shaped pin tip about 3.5 mm to the right of the edge.

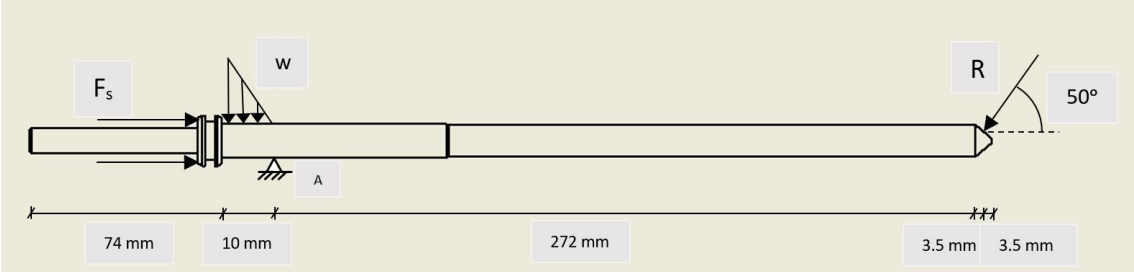

Figure 3.8: Free-body diagram of the pin when the tip angle is 40°.

Chapter 4

Results

4.1 Material Selection for the Seal Retainer

Table 4.1 shows the top-ranked stainless steels based on price (alloy surcharges) and yield strength. Only the stainless steels with sufficient yield strength were included. All the stainless steels had martensitic structure after oil quenching and tempering, except for EN 1.4568 which was precipitation hardened [6]. The third column from the left in Table 4.1, is determined by Eq. 3.1. as mentioned in section 3.2. Eq. 3.1 was used to determine a number which was used to rank the commercially available stainless steel grades. Hence, the aim was to determine the grades with the lowest number in the middle column of Table 4.1.

Ranking	EN Steel Grade	Alloy Surcharges over Yield Strength	Yield Strength [MPa]	Alloy Surcharges [kr/tonne]
1	1.4034	3.45	1480	5109.2
2	1.4110	5.01	1330	6669.9
3	1.4419	5.95	1240	7129.5
4	1.4057	6.80	1100	7478.7
5	1.4568	8.15	1580	12888.9

Table 4.1: Stainless steel ranking [1], [2], [3], [4], [5], [6].

The proposed stainless steel has the EN grade 1.4034 (Europe) and ASTM grade 420 (USA). It has excellent mechanical properties in combination with a low price.

4.2 Tip Angle Optimization

Table 4.2 shows the deviation between the maximum shear stresses determined by numerical (FEM)- and analytical method when using the design pressure.

Case	FEM τ_{max} [MPa]	Analytic τ_{max} [MPa]	Deviation between FEM and Analytical
1	3328.5	3124.4	204.1 MPa / 6.5%
2	503.5	354.7	148.8 MPa / 41.9%
3	3119.5	3258.9	139.4 MPa / 4.3%

Table 4.2: Deviations between analytical- and numerical maximum shear stresses.

Table 4.3 shows the maximum shear stresses by numerical- and analytical methods. In addition, the utilization of two different methods would act as validation. The far-right column shows the maximum allowable shear stress according to the Tresca criterion, which is half of the steel's yield strength. The steel that is considered here is EN 1.4034, which is the top-ranked stainless steel.

Case	Tip Angle [°]	FEM τ_{max} [MPa]	Analytic τ_{max} [MPa]	Y/2 [MPa]
1	45	3328.5	3124.4	740
2	40	503.5	354.7	740
3	35	3119.5	3258.9	740

Table 4.3: Summary of the tip optimization.

The analytical contact stresses are shown in Table 4.4. Case 1 is analysed using two different edge radii in order to indicate the large impact of the edge radius for tip angles above 40°. Hence, case 1 is split into case 1a and case 1b, which has the maximum and half of the maximum allowable edge radii respectively.

Case	Tip Angle [°]	Edge Radius [mm]	τ_{max} [MPa]
1a	45	0.6 (max. allowable)	3124.4
1b	45	0.3	4047.8
2	40	0.6 (max. allowable)	354.7
3	35	0.6 (max. allowable)	3258.9

Table 4.4: Analytical results for tip angle contact stresses.

The numerical maximum contact stresses from ANSYS analysis with force in the vertical direction and ambient temperature of 22 °C are shown in Table 4.5. It is a conservative estimate and the most comparable with the analytical solution.

Case	Tip Angle [°]	τ_{max} [MPa]	Max. von-Mieses [MPa]
1	45	3328.5	6253.9
2	40	503.5	931.9
3	35	3119.5	6207.2

Table 4.5: ANSYS analysis with vertical force.

The numerical maximum contact stresses from ANSYS analysis with force in the axial direction and ambient temperature of 22 °C are shown in Table 4.6.

Case	Tip Angle [°]	$\tau_{\max}$ [MPa]	Max. von-Mieses [MPa]
1	45	2364.1	4472.2
2	40	338.4	628.2
3	35	3019.8	6010.1

Table 4.6: ANSYS analysis with axial force.

The numerical maximum contact stresses from ANSYS analysis with force in the axial direction and the minimum ambient temperature of 2 °C are shown in Table 4.7.

Case	Tip Angle [°]	$\tau_{\max}$ [MPa]	Max. von-Mieses [MPa]
1	45	2372.2	4483.7
2	40	370.6	693.0
3	35	3053.1	6077.0

Table 4.7: ANSYS analysis with axial force and constant 2 °C.

The numerical maximum contact stresses from ANSYS analysis with force in the axial direction and the maximum ambient temperature of 149 °C are shown in Table 4.8.

Case	Tip Angle [°]	$\tau_{\max}$ [MPa]	Max. von-Mieses [MPa]
1	45	2330.4	4406.7
2	40	271.0	524.9
3	35	2820.9	5596.6

Table 4.8: ANSYS analysis with axial force and constant 149 °C.

4.3 Bending, Buckling and Axial Loading

The maximum bending stress for the pin is located near o-ring 1. The value of the maximum bending stress is 1064.5 MPa with the current pin with a 45° tip angle. The maximum bending stress is 1078.2 MPa with the proposed 40° tip angle. The design pressure is used for calculating all the stresses as mentioned earlier.

The maximum normal stress for the pin is equal to 5.8 MPa. The critical axial force is equal to 162.1 kN.

The critical buckling force is equal to 25.7 kN for 45° tip angle and 25.1 kN for 40° tip angle.

4.4 Contact Stresses on the Housing

The maximum shear stress in the housing is 224.9 MPa.

4.5 Acceptance of the Seal Retainer

Table 4.9 shows the maximum shear stresses on the housing and the pin when using the design pressure. A tip angle of 40° is used. The maximum shear stress in the pin is equal to that of the seal. Half of the yield strength must be higher than the maximum shear stresses in order to satisfy Tresca's requirement. Since half of the yield strength is higher than the maximum shear stresses, the requirement is fulfilled for a 40° tip angle.

Contact Stresses on housing [MPa]		**Contact Stresses on pin (Analytic) [MPa]**		**Contact Stresses on pin (Numerical) [MPa]**	
$\tau_{\mathbf{max}}$	**Y/2**	$\tau_{\mathbf{max}}$	**Y/2**	$\tau_{\mathbf{max}}$	**Y/2**
224.9	740	354.7	740	503.5	740

Table 4.9: Summary of the contact stresses for 40° tip angle.

Table 4.10 shows the maximum bending stress, maximum axial stress, critical buckling force and the critical axial force for 40° tip angle. The critical buckling force and the critical axial force is much higher than the load. Hence, buckling and compression of the pin will not occur. The maximum bending stress and maximum axial stress is fulfilling the requirement of being less than the yield strength. However, the maximum bending stress of the pin is quite high while still in no risk of yielding or failure. The maximum bending stress is high because the pin is long and thin. The safety factor for bending stress using the design pressure is 1.39 if the suggested stainless steel is utilized. If the operational pressure is used, the force would be 32.3% lower. The operational pressure will result in a safety factor of 2.05, which indicates that the tool is operationally safe with a sufficient margin.

Bending Stress [MPa]		**Axial Loading Stress [MPa]**		**Critical Buckling Force [kN]**	**Critical Axial Force [kN]**
$\sigma_{\mathbf{b,max}}$	**Y**	$\sigma_{\mathbf{n,max}}$	**Y**		
1078.2	1480	5.8	1480	25.1	162.1

Table 4.10: Stresses and critical forces for 40° tip angle.

Chapter 5

Discussion

5.1 Stainless Steel Selection for the Retainer

All the stainless steels with the lowest alloy surcharges had low amounts of alloying elements in general. However, all stainless steels has additions of chromium since it increases the corrosion resistance. High amounts of chromium content is in fact what separates a stainless steel from a regular steel. Chromium aid in forming a thin oxide layer on the surface, which is why stainless steels have increased corrosion resistance compared to regular steels [12]. Chromium is priced around half the price of nickel, and is a very expensive alloy. However, prices of the alloying ores experience fluctuations on a daily basis. The fluctuations are comparable to stocks on the stock markets. The most expensive alloying elements used in stainless steels are molybdenum, nickel and chromium. High amounts of expensive alloys will directly result in expensive steels.

The metal that is being used for the retainer today is Inconel 718. The metal has 50–55% nickel, 17–21% chromium and 2.8–3.3% molybdenum [9]. Hence, the total content of nickel, chromium, and molybdenum is 69.8–79.3%. This indicates that the most expensive alloys make up most of the mass in Inconel 718. This is why the metal that is being used today is so expensive.

The suggested stainless steel is EN 1.4034, which has 0.43–0.50% carbon and 12.5–14.5% chromium [13]. Hence, the amount of expensive alloys are at its bare minimum. It is therefore amongst the most inexpensive stainless steels on the market. Due to its relatively high amounts of carbon, the steel has high hardenability. The steel is often quenched and tempered to reach yield strengths of 1480 MPa with martensite structure [14]. The corrosion resistance is optimized when the steel is both hardened and has a polished surface finish [15]. It has good corrosion resistance in water and other moderately corrosive environments [15]. The seal retainer also has a protective coating, which increases its corrosion resistance.

5.2 Steel Structures and Treatments

The most widely used steel structures includes ferrite, austenite, duplex and martensite. Martensite structures are the strongest and can only be achieved by rapid cooling rates e.g. water- or oil quenching [12]. Martensitic steels are often the most brittle. However, stainless steels are alloyed. The alloying elements may push the TTT diagram nose so that slower cooling mediums e.g. oil quenching or even air cooling can be used to form a martensitic structure [12]. Slower cooling rates and higher tempering temperatures result in more ductile steels [12]. However, higher tempering temperatures will generally result in lower strength [12]. Hence, one attribute will often limit another attribute.

5.3 Martensitic Stainless Steel

The strength of martensite stainless steel is highly dependent on the condition. Steels in annealed condition have as low as 275 MPa yield strength, while steels in quenched and tempered condition can have as high as 1900 MPa [16]. Martensitic stainless steels are often used when high strength and corrosion resistance are needed [12]. Martensitic stainless steels can be grouped into four groups [17]. The first group are Fe-Cr-C steels, which have high hardenability, high strength and low cost, but have lower corrosion resistance compared to the other groups [17]. The Fe-Cr-C steels are the best fit for the retainer, and the molybdenum disulfide coating will increase the corrosion resistance along with hardening of the steel. EN 1.4034 and EN 1.4125 are Fe-Cr-C steels. EN 1.4125 steel was not included in the alloy surcharges analysis as it could not be found. However, it is assumed that EN 1.4125 has low alloy surcharges because the chemical composition is very similar to that of EN 1.4034. Thus, the prices are assumed to be almost identical. Molybdenum additions can increase the corrosion resistance, but it has a high cost. If higher corrosion resistance is required, then group 2 or 3 steels can be considered. Group 2 steels replaces parts of carbon with the addition of expensive nickel [17]. Group 3 steels has even higher amounts of expensive alloys e.g. nickel, molybdenum and chromium [17]. Group 3 steels are often used for aerospace and other extremely demanding applications [17]. Group 4 steels has relatively low amounts of chromium, but have good creep resistance in temperatures up to 650 °C [17]. All the martensitic stainless steels are normally not suitable for cryogenic environments, and many of them can also become brittle in environments with temperatures above 430 °C [16]. The retainer is operating in the range between 2 °C and 149 °C, so very extreme temperatures will not be a challenge that the retainer has to face.

5.4 Effects of Alloying Elements in Stainless Steels

Alloying elements affects steel in many ways. There are over a hundred commercial stainless steels with an unique mixture of alloying elements. The aim of each mixture is to fulfill certain functions. Some of the functions may be more general in nature e.g. high strength or high corrosion resistance, while others may be more specific e.g. audio-frequency. For the retainer, high hardenability, high strength, high corrosion resistance and low cost are some of the most important factors.

5.5 Sulphur Additions in Stainless Steels

Lower pitting potentials mean decreased corrosion resistance. The pitting potential decreases with higher contents of sulphur. Sulphur additions contain sulphide inclusions with very low corrosion resistance [18]. Sulphur additions will compromise the function of chromium in stainless steels. Hence, stainless steels with sulphur contents should be avoided.

5.6 Seal Retainer

The seal retainer consists of multiple components i.e. pin, housing, cap, o-rings, and a spring. The seal retainer is used to hold and release a seal in a subsea environment. The retainer is interfaced with the Master Valve Block (MVB), which is located up to 500 m below the water surface. The MVB is located inside the assemblies of equipment called Christmas trees at the oil wellheads. The temperatures vary from a minimum of 2 °C to a maximum of 149 °C. The design life of the retainer is 25 years, but it will be delivered to service every seven years because of the life expectancy of the o-rings. The coating of the seal retainer is molybdenum disulphide, MoS2 coating. Figure 5.1 shows the seal retainer from the connector side on the left. A technical drawing of the re-designed seal retainer is included in the appendix.

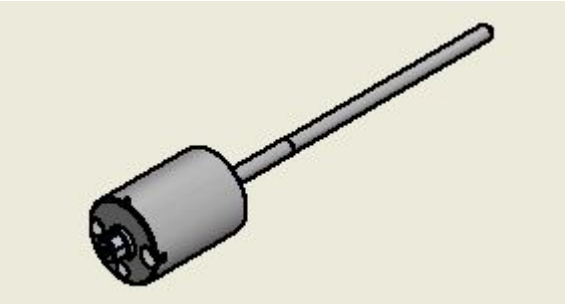

Figure 5.1: Seal Retainer.

The retainer is interfaced with two bolt connections to the MVB. The retainer is currently in Inconel 718 material. A total of four retainers are installed to retain each seal. The proposal is to change the material of the retainer to EN 1.4034 or possibly a similar high strength and low cost stainless steel.

5.7 Seal

The seal is held in place by a total of four seal retainers. During installations, the retainers release the seal. Figure 5.2 shows the geometry of the seal. The material of the seal is 17-4PH (UNS S17400), which is a very strong material.

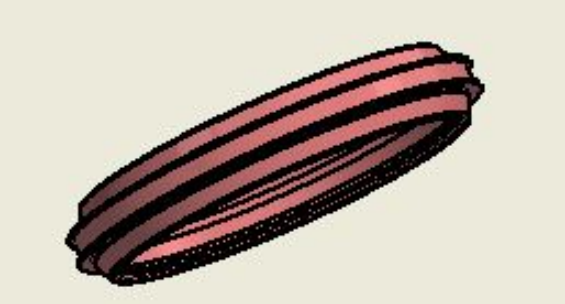

Figure 5.2: Seal.

5.8 Pin

The function of the pin is to hold the seal in place. The tip angle is an important factor for seal holding. The tip angle of the seal is to be optimized for minimum contact stresses between the two bodies. The tip angle is currently 45°, and the proposal is to change it to 40°. Figure 5.3 shows a overview of the pin, and the tip of the pin is located at the far right in the figure. The pin is both long and thin, which makes it prone to bending. The diameter is 11.81 mm close to the tip, and 12.5 mm where the highest bending moment is located. A larger diameter will decrease the bending stress, so it is wise to have the larger diameter where the maximum bending moment is. There is also a possibility of increasing the diameter of the pin, which would decrease the bending stress further. Equation 5.1 shows the relationship between the bending stress σ_b, the bending moment M_b, and the pin diameter d.

$$\sigma_b = \frac{M_b}{\frac{\pi d^3}{32}} \tag{5.1}$$

The pin diameter is to the power of three in the denominator. Hence, increasing the pin diameter by a factor of 2 will e.g. decrease the bending stress by a factor of 8. There is a possibility of e.g. increasing the pin diameter where it is 12.5 mm to 13.0 mm. The increase of 0.5 mm in diameter would result in a decrease of maximum bending stress by 118.2 MPa. One can, for example, also increase the pin diameter where it is 11.81 mm to a higher diameter. That would simultaneously decrease the contact stresses between the pin tip and the seal if the tip angle is changed to 40°. The contact stresses between the pin and the seal would slightly decrease because the line contact between the two bodies would have an increased distance. Thus, there are multiple simple measures that can be taken to reduce the most high-risk stresses. Reducing some of the maximum stresses will lead to a decreased requirement of strength for the materials. However, no size adjustments are necessary with the proposed tip angle and material. The design pressure was used as mentioned earlier, and every analysis resulted in sufficient safety margins.

Figure 5.4 shows the dimensions of the re-designed optimal retainer pin. The only difference between the optimal pin and the current pin is the tip angle. The tip angle for the optimal pin is 40°, and the current pin has a 45° tip angle. The optimal tip angle of the pin is magnified in detail A at the lower right corner of Fig. 5.4. The proposed stainless steel is also listed at the top in Fig. 5.4.

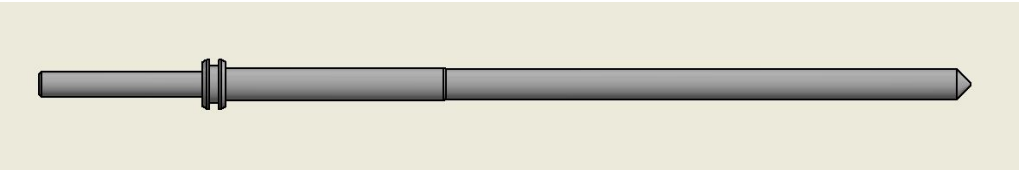

Figure 5.3: Overview of the current pin used for seal retainers today.

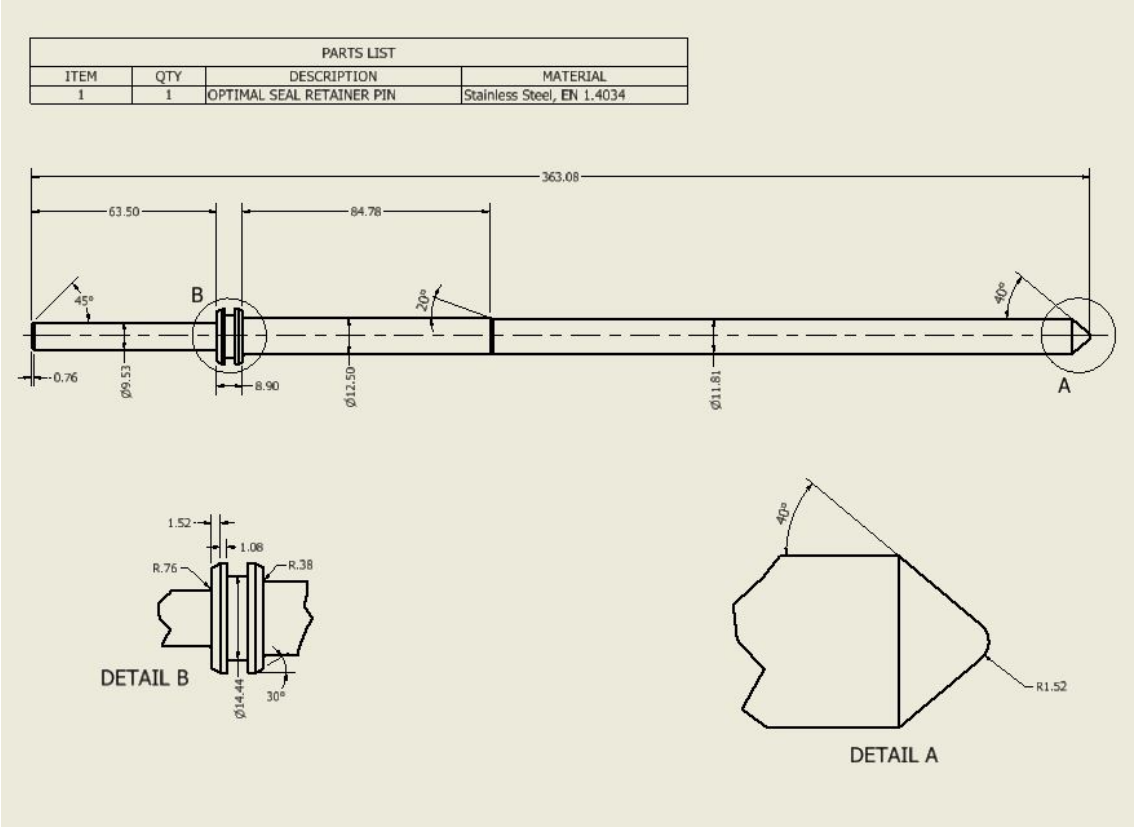

Figure 5.4: The dimensions of the re-designed optimal seal retainer pin.

5.9 Housing

The housing is interfaced toward the Master Valve Block (MVB) with two bolts. The housing functions as a pin holder. The housing also has a hydraulic fluid chamber which is connected near the o-rings. Figure 5.5 shows the geometry of the housing. The assembly drawing in the appendix shows more details of the housing.

5.10 Spring

The spring is connected between the pin and the cap. The spring is never in a neutral position, it is always compressed. The spring will compress further and pull the pin away from

Figure 5.5: Housing.

the seal when the hydraulics are activated. The spring is static during normal operation. Figure 5.6 shows the geometry of the spring.

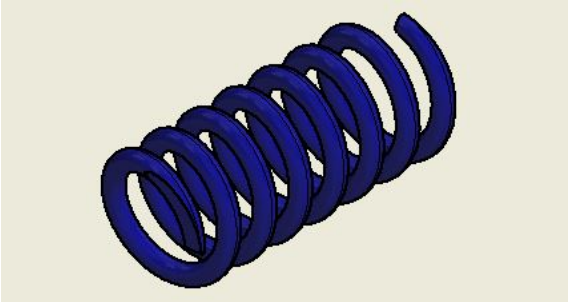

Figure 5.6: Spring.

5.11 Cap

The cap is both connected to the spring and the housing. The cap works as a wall in restricting movement of the spring so that the spring can push the pin towards the seal. Figure 5.7 shows the geometry of the cap.

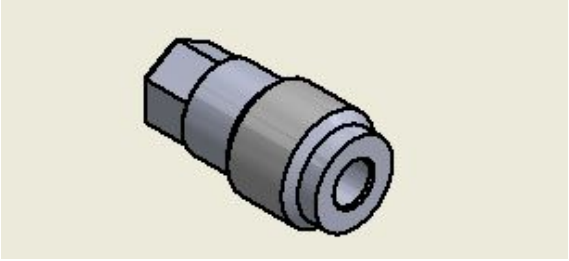

Figure 5.7: Cap.

5.12 O-rings

The function of the o-rings is to seal certain areas when the hydraulic fluid pressure pulls the pin away from the seal during activation. Both of the o-rings are located in grooves enclosed by the housing. The grooves restricts the o-rings from moving out of position in the axial direction. The hydraulics will be activated during installations. Installations does not occur often at subsea. The o-rings sits in an environment without sunlight, and will typically have a life expectancy of approximately 7 years. However, there is no certainty of exactly how long the o-rings will function in this environment. The o-rings operate together with fluid pressure from a fluid chamber to compress the spring further. This occurs inside the housing of the retainer. The working pressure is 4.2 MPa and the design pressure is 6.2 MPa. The design pressure is used during the analysis. Figure 5.8 shows the toroid-shaped o-rings.

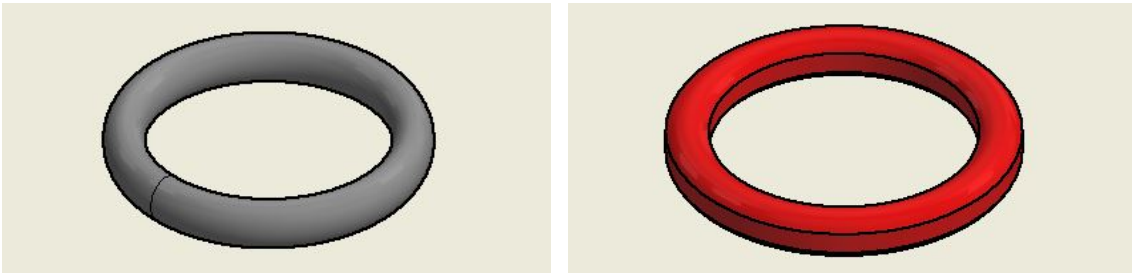

(a) O-ring 1 **(b)** O-ring 2

Figure 5.8: Overview of the o-rings.

5.13 Tip Angle Optimization Case 1

Figures 5.9–5.12 show the shear stresses between the pin tip and the seal. The figures show the cross-sectional view 'section 1', which is explained by Fig. 3.6a. The contact stresses (shear stresses) around the point contact is shown. The figures in section 5.13 are from case 1, which has a 45° tip angle. The contact stresses have similar values to case 3, and much higher than case 2. The maximum shear stress in the simulations of case 1 ranges from about 2300 MPa to about 3300 MPa, which is very high. There is a high risk of yielding or failure with the high shear stresses. Hence, tip angles of around 45° should not be used. The sharp edge will cause high contact stresses.

Figure 5.9 shows the shear stress distribution for vertical force and an ambient temperature of 22 °C. The pin and the seal are deformed by the high contact stresses. The maximum shear stress is 3328.5 MPa, which is the highest of all the simulations for case 1.

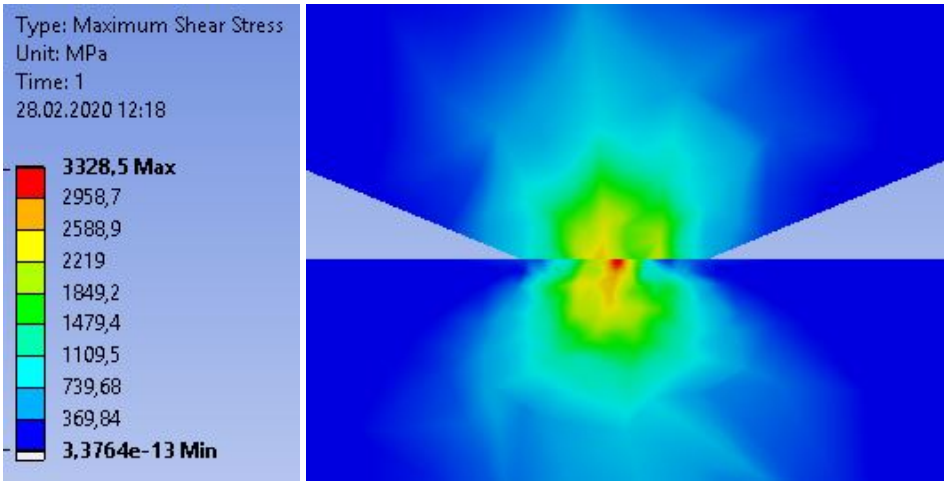

Figure 5.9: Cross-sectional view of 'section 1' for case 1 with vertical force.

Figure 5.10 shows the shear stress distribution for axial force and an ambient temperature of 22 °C. The pin and the seal are deformed by the high contact stresses. The maximum shear stress is 2364.1 MPa, which is lower than the vertical force simulation. The relatively large difference between the vertical force and the axial force is due to the installation angle and the geometry of the pin.

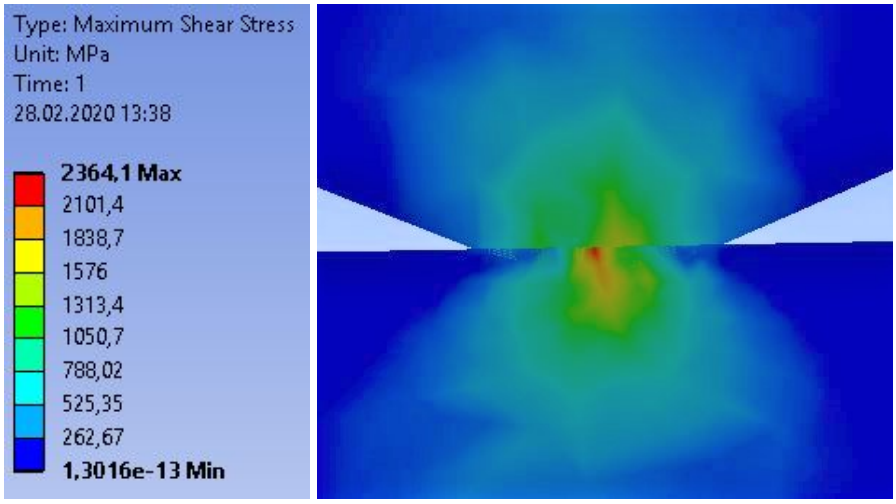

Figure 5.10: Cross-sectional view of 'section 1' for case 1 with axial force.

Figure 5.11 shows the shear stress distribution for axial force and the minimum ambient temperature of 2 °C. The pin and the seal are deformed by the high contact stresses. The maximum shear stress is 2372.1 MPa, which is higher than the simulation with the highest temperature. Hence, the lowest temperature resulted in slightly higher contact stresses compared to the highest temperature.

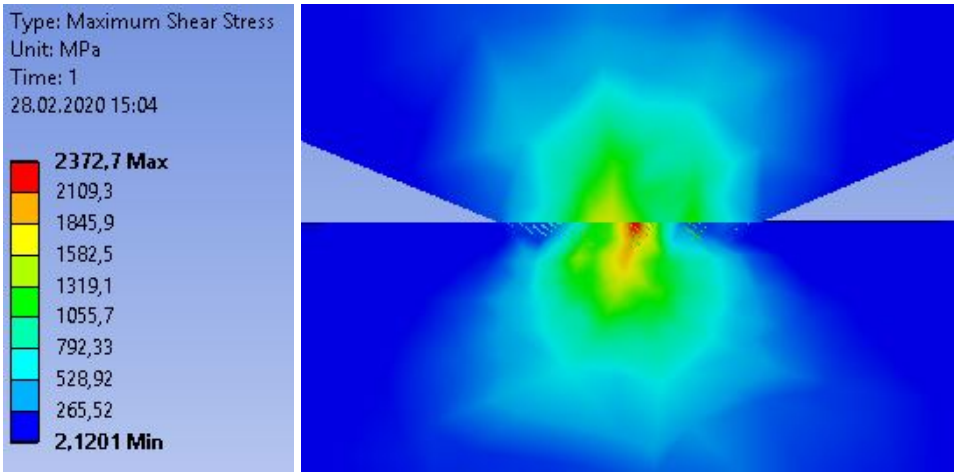

Figure 5.11: Cross-sectional view of 'section 1' for case 1 with axial force and 2°C.

Figure 5.12 shows the shear stress distribution for axial force and the maximum ambient temperature of 149 °C. The pin and the seal are deformed by the high contact stresses. The maximum shear stress is 2330.4 MPa, which was the lowest shear stress of all the simulations for case 1.

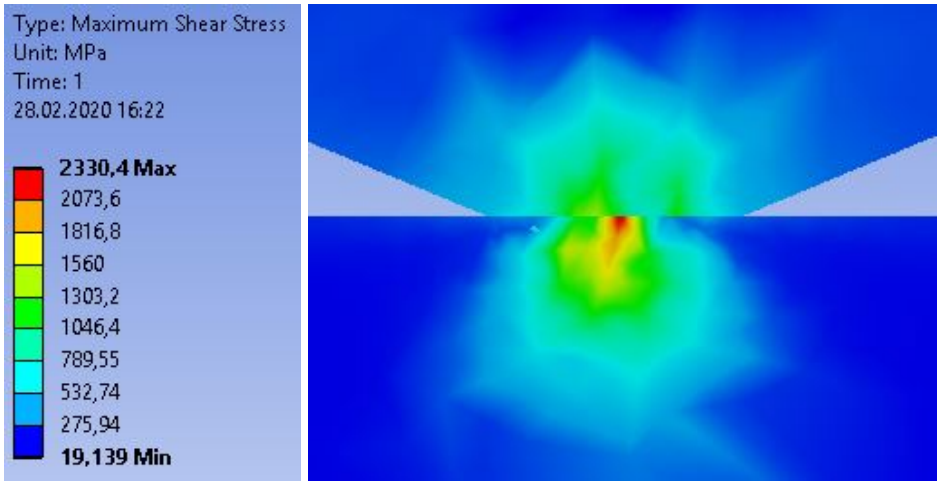

Figure 5.12: Cross-sectional view of 'section 1' for case 1 with axial force and 149°C.

5.14 Tip Angle Optimization Case 2

Figures 5.13–5.16 show the shear stresses between the pin tip and the seal. The figures show the cross-sectional view 'section 1', which is explained by Fig. 3.6a. The contact stresses around the line contact are shown. The line contact results in far lower shear stresses in case 2 compared to the other cases. All the figures in section 5.14 are from case 2, which has a 40° tip angle. The maximum shear stress in the simulations of case 2 ranges from about 270 MPa to about 500 MPa, which is relatively low. There is low risk of yielding or failure with a tip angle of 40°. A martensitic stainless steel with a yield strength of minimum 1000 MPa will handle these shear stresses.

Figure 5.13 shows the shear stress distribution for vertical force and an ambient temperature of 22 °C. The maximum shear stress is 503.5 MPa, which is the highest of all the simulations for case 2.

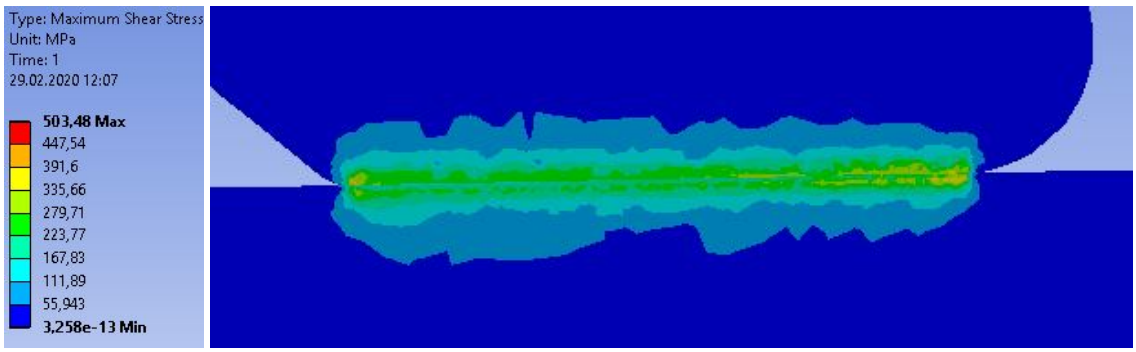

Figure 5.13: Cross-sectional view of 'section 1' for case 2 with vertical force.

Figure 5.14 shows the shear stress distribution for axial force and an ambient temperature of 22 °C. The maximum shear stress is 338.4 MPa, which is lower than the vertical force simulation.

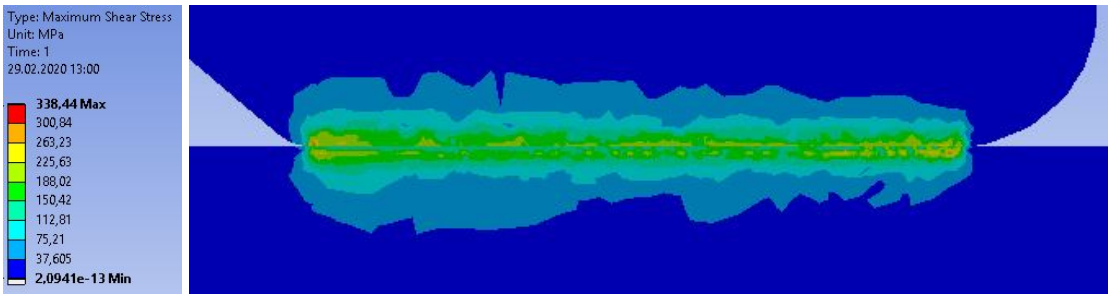

Figure 5.14: Cross-sectional view of 'section 1' for case 2 with axial force.

Figure 5.15 shows the shear stress distribution for axial force and the minimum ambient temperature of 2 °C. The maximum shear stress is 370.1 MPa, which is higher than the simulation with the highest temperature. Hence, the lowest temperature resulted in higher contact stresses compared to the highest temperature.

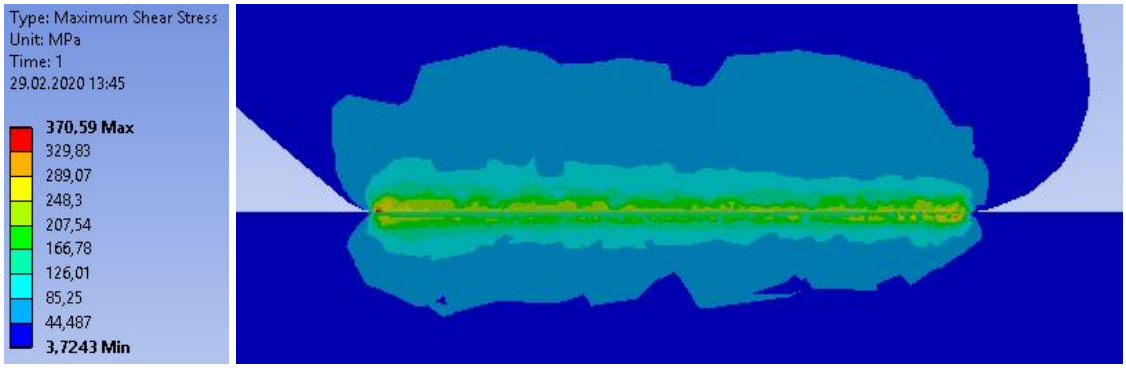

Figure 5.15: Cross-sectional view of 'section 1' for case 2 with axial force and 2°C.

Figure 5.16 shows the shear stress distribution for axial force and the maximum ambient temperature of 149 °C. The contact stresses was lower than the stresses around the fixed support of the seal in this situation. Hence, the contact stresses had to be manually probed in order to be determined. The probing showed a maximum shear stress of about 271 MPa, which was the lowest shear stress of all the simulations for case 2.

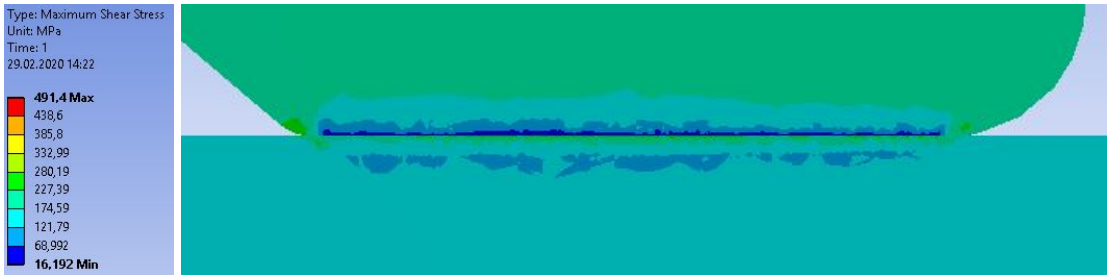

Figure 5.16: Cross-sectional view of 'section 1' for case 2 with axial force and 149°C.

5.15 Tip Angle Optimization Case 3

Figures 5.17-5.20 show the shear stresses between the pin tip and the seal. The figures show the cross-sectional view 'section 2', which is explained by Fig. 3.6b. The contact stresses (shear stresses) around the point contact is shown. The figures in section 5.15 are from case 3, which has a 35° tip angle. The contact stresses have similar values to case 1 and far higher than case 2. The maximum shear stresses in the simulations of case 3 are approximately 3000 MPa, which is very high. There is a high risk of yielding or failure with the high shear stresses. Hence, tip angles of around 35° should not be used.

Figure 5.17 shows the shear stress distribution for vertical force and an ambient temperature of 22 °C. The pin and the seal are deformed by the high contact stresses. The maximum shear stress is 3119.5 MPa, which is the highest of all the simulations for case 3.

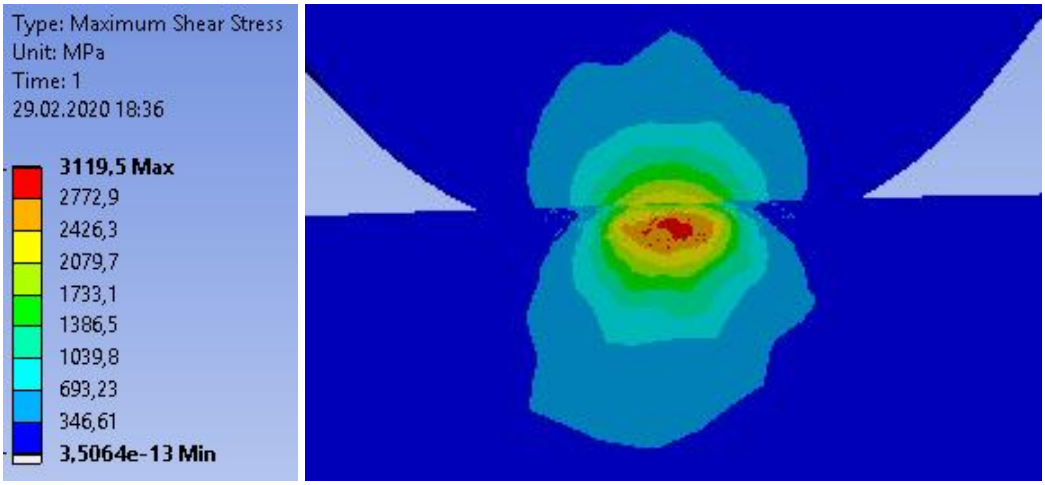

Figure 5.17: Cross-sectional view of 'section 2' for case 3 with vertical force.

Figure 5.18 shows the shear stress distribution for axial force and an ambient temperature of 22 °C. The pin and the seal are deformed by the high contact stresses. The maximum shear stress is 3019.8 MPa, which is lower than the vertical force simulation.

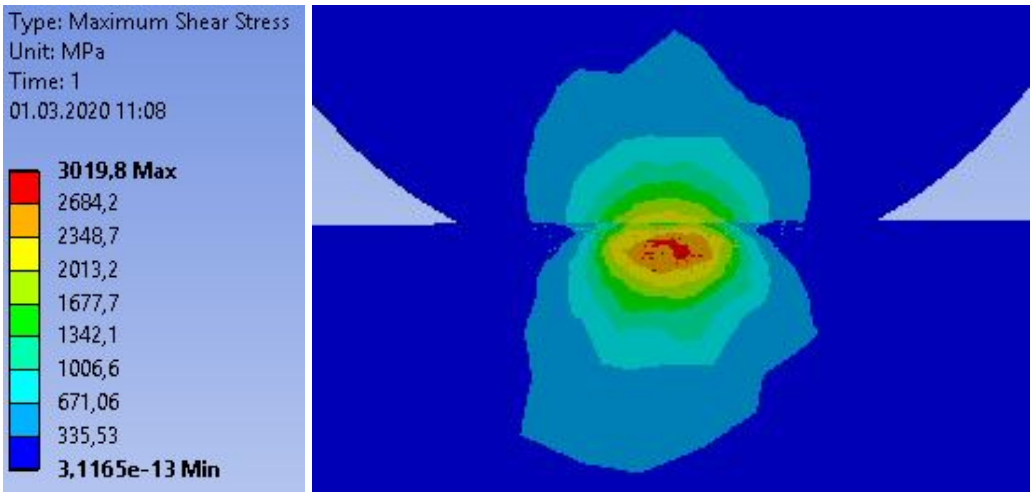

Figure 5.18: Cross-sectional view of 'section 2' for case 3 with axial force.

Figure 5.19 shows the shear stress distribution for axial force and the minimum ambient temperature of 2 °C. The pin and the seal are deformed by the high contact stresses. The maximum shear stress is 3053.1 MPa, which is higher than the simulation with the highest temperature. Hence, the lowest temperature resulted in higher contact stresses compared to the highest temperature.

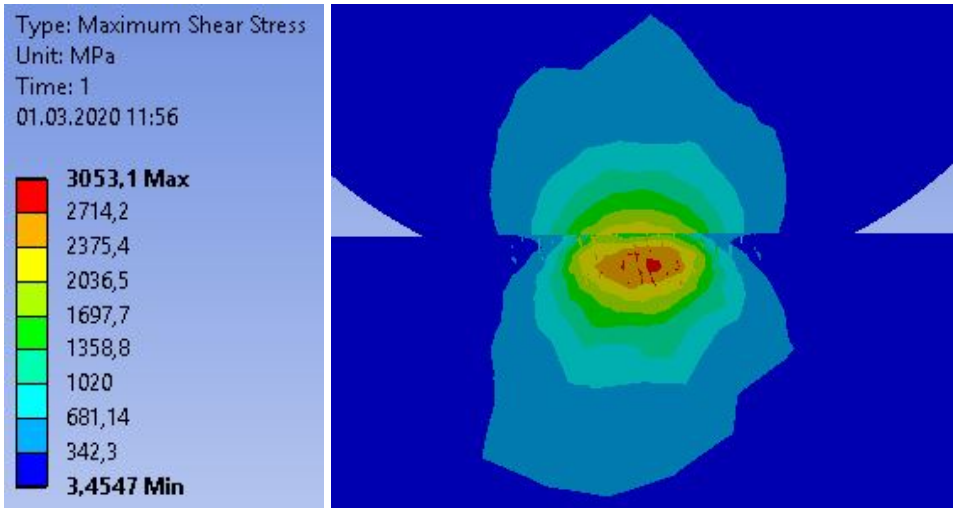

Figure 5.19: Cross-sectional view of 'section 2' for case 3 with axial force and 2°C.

Figure 5.20 shows the shear stress distribution for axial force and the maximum ambient temperature of 149 °C. The pin and the seal are deformed by the high contact stresses. The maximum shear stress is 2820.9 MPa, which was the lowest shear stress of all the simulations for case 3.

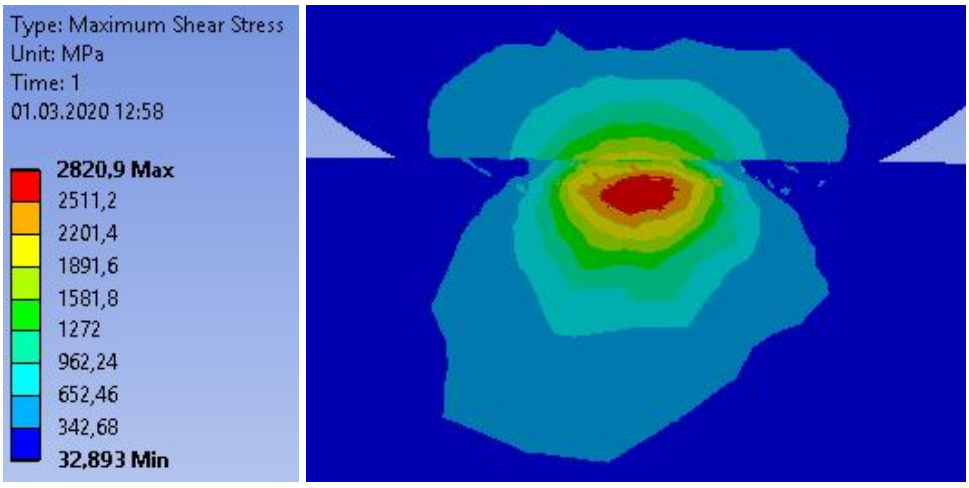

Figure 5.20: Cross-sectional view of 'section 2' for case 3 with axial force and 149°C.

Chapter 6

Conclusion

6.1 Stainless Steel Selection for the Retainer

The most appropriate choice of stainless steel for the retainer is EN 1.4034. The martensitic steel has excellent mechanical properties and good corrosion resistance in moderately corrosive environments. It is also amongst the most inexpensive stainless steels due to relatively low amounts of alloying elements. The steel has no nickel or molybdenum, which are the most expensive alloys. The current material, Inconel 718, has very high amounts of the most expensive alloying elements. In addition, the prices of nickel and molybdenum are prone to value fluctuations, which can lead to even higher material costs. The proposed stainless steel grade only has the necessary alloying elements with the appropriate contents. The current steel has non-essential alloying elements, and also high quantities of these alloys.

Advantages of using EN 1.4034:

- Substantially lower material costs resulting in much cheaper seal retainers.
  - 69.8–79.3% of the total mass in the current material consists of the most expensive alloying elements.
  - Only 12.5–14.5% of the total mass in the proposed stainless steel consists of the most expensive alloying elements.
  - 50–55% nickel in the current material.
  - No additions of nickel in the proposed stainless steel.
  - 2.8–3.3% molybdenum in the current material.
  - No additions of molybdenum in the proposed stainless steel.
  - 17–21% chromium in the current material.
  - 12.5–14.5% chromium in the proposed stainless steel.
- Excellent mechanical properties.

  - Yield strengths of around 1500 MPa can be achieved by oil quenching and tempering of the proposed stainless steel.
  - The mechanical properties are suitable for the application.

- The functionality of the retainer will be maintained.
  - The proposed material can perform the same tasks efficiently.

- Sufficient corrosion resistance when the current coating is used.
  - The chromium content gives high corrosion resistance.
  - The protective coating gives additional corrosion protection.

- Steadier alloy prices.
  - Lower amounts of rare alloying elements.
  - Rare alloying elements can experience large price fluctuations.

- Only the necessary alloying elements are used.
  - Using a suitable chemical composition for the specific application.

Disadvantages of using EN 1.4034:

- Lower corrosion resistance compared to the current material.
  - The proposed stainless steel has 2.5–8.5% lower amounts of chromium content compared to the current material.
  - The proposed stainless steel has no additions of nickel and molybdenum.

- There will be some initial investment cost associated to changing the material.
  - Costs related to ordering of a new material.
  - Costs related to decreased order size.
  - Costs related to the implementation of a new material.
  - Administration costs.

The proposed stainless steel grade EN 1.4034 is the best alternative for Aker Solutions as they aim for reducing costs and maintaining the functionality of the tool. The other suggested stainless steel grades will also reduce the material costs of the seal retainer compared to the current material being used. Changing the current material of the seal retainer has great potential.

6.2 Tip Angle Optimization

The tip angle that results in the lowest amount of contact stresses is 40°. The result of a 40° tip angle is a line contact between the pin and the seal. All other tip angles will result in point contacts between the two components. With a line contact causing lower contact stresses, there will be less damage on the pin and the seal. Hence, the proposal is to change the tip angle from 45° to 40° for optimal design life and safety for the retainer and the seal. Figure 5.4 shows the 40° tip angle of the pin.

Advantages of 40° tip angle:

- Much lower contact stresses on the retainer and the seal.
  - Line contact is superior compared to point contacts.
  - The maximum shear stress will decrease by about 90 %.
- Less deterioration and damage on the retainer and the seal.
  - Lower contact stresses results in less damage.
  - Both the seal retainer and the seal will have lower contact stresses and increased design life.
- Lower risk of failure.
  - Increased safety.
  - With lower contact stresses, the probability of failure decreases.

Disadvantages of 40° tip angle:

- Negligibly higher bending stresses.
  - Increase of about 1 %.
- There will be some initial investment cost associated to changing the tip angle.
  - Costs related to the change in design.
  - Costs related to the change in machine programming.
  - Administration costs.

6.3 Further Research

Future studies can, for example, include corrosion experiments with coated steels in seawater. The aim of such experiments are to determine the corrosion rates of various steels with various protective coatings. The corrosion rates from the experiments can be used to determine the design life of various tools such as the seal retainer. For the first experiment, the proposed stainless steel grade EN1.4034 can be compared against the current material of the seal retainer Inconel 718. Both materials would have the molybdenum disulphide (MoS2) coating, which is currently being used for the seal retainer. Both experimental

bodies could rest in seawater pools over a certain period of time. Afterward, measurements can be obtained to determine the corrosion rates of both bodies. Such experiments could also be done without protective coating to save time.

There is also a possibility of performing an experiment to determine whether there is electrical conductivity in the seal retainer. The aim of the experiment is to determine whether or not sacrificial anodes can be used instead of protective coating for the seal retainers. The hypothesis can e.g. be that there is not an electrical conductivity, because the housing is resting on the polymer o-rings of the pin, which are non-magnetic.

Bibliography

[1] Outokumpo, "Stainless steel alloy surcharges europe," accessed: 02.03.2020. [Online]. Available: https://www.outokumpu.com/ja-jp/surcharges/stainless-steel-alloy-surcharges-europe

[2] W. Material, "Ss420 grade aisi 420 stainless steel properties, heat treatment, hardness, magnetic," accessed: 05.03.2020. [Online]. Available: https://www.theworldmaterial.com/ss420-astm-aisi-420-stainless-steel-grade/

[3] MakeitFrom, "Quenched and tempered (+qt) 1.4110 stainless steel," accessed: 06.03.2020. [Online]. Available: https://www.makeitfrom.com/material-properties/Quenched-and-Tempered-QT-1.4110-Stainless-Steel

[4] MakeItFrom, "Quenched and tempered (+qt) 1.4419 stainless steel," accessed: 06.03.2020. [Online]. Available: https://www.makeitfrom.com/material-properties/Quenched-and-Tempered-QT-1.4419-Stainless-Steel

[5] MakeitFrom, "Hardened (h) 431 stainless steel," accessed: 07.03.2020. [Online]. Available: https://www.makeitfrom.com/material-properties/Hardened-H-431-Stainless-Steel

[6] Virgamet, "17-7ph, x7crnial17-7, 1.4568, uns s17700 - stainless steel," accessed: 07.03.2020. [Online]. Available: https://virgamet.com/17-7ph-x7crnial177-1-4568-aisi-631-uns-s17700-stainless-steel

[7] A. Boresi and R. Schmidt, *Advanced Mechanics of Materials*. John Wiley & Sons, 2003. [Online]. Available: https://books.google.no/books?id=KcAjIQAACAAJ

[8] M. Stahl, "Alloy subcharge," accessed: 27.03.2020. [Online]. Available: https://www.montanstahl.com/blog/alloy-surcharge/

[9] S. Metals, "Inconel alloy 718," accessed: 15.03.2020. [Online]. Available: https://www.specialmetals.com/assets/smc/documents/inconel_alloy_718.pdf

[10] Ansys, Inc., "Ansys academic research licence," software program, version 2019R3. [Online]. Available: https://www.ansys.com/

[11] Autodesk, “Inventor professional,” software program version 2020.0.1. [Online]. Available: https://www.autodesk.no/products/inventor/overview

[12] H. Bhadeshia and R. Honeycombe, *Steels: Microstructure and Properties*. Elsevier Science, 2017. [Online]. Available: https://books.google.no/books?id=4Rt5CgAAQBAJ

[13] Standard, “En 10088-2 stainless steels - part 2: Technical delivery conditions for sheet/plate and strip of corrosion resisting steels for general purposes,” European Committee for Standardization, Brussels, Belgium, Standard, Jun. 2005.

[14] T. W. Material, “Ss420 grade aisi 420 stainless steel properties, heat treatment, hardness, magnetic,” accessed: 05.03.2020. [Online]. Available: https://www.theworldmaterial.com/ss420-astm-aisi-420-stainless-steel-grade/

[15] D. S. D. Edelstahlwerke, “1.4034,” accessed: 04.03.2020. [Online]. Available: https://www.dew-stahl.com/fileadmin/files/dew-stahl.com/documents/Publikationen/Werkstoffdatenblaetter/RSH/1.4034_en.pdf

[16] W. Garrison Jr and M. Amuda, “Stainless steels: Martensitic,” *Encyclopedia of Materials: Science and Technology*, 2017, accessed: 19.03.2020.

[17] Rowe and Heritier, “Martensitic stainless steels,” accessed: 20.03.2020. [Online]. Available: https://www.worldstainless.org/Files/issf/non-image-files/PDF/ISSF_Martensitic_Stainless_Steels.pdf

[18] I.-S. L. Y.-S. P. Soon-Hyeok Jeon, Soon-Tae Kim, “Effects of sulfur addition on pitting corrosion and machinability behavior of super duplex stainless steel containing rare earth metals: Part 2,” *Corrosion Science*, vol. 52, no. 10, pp. 3537–3547, Oct. 2010, accessed: 18.03.2020. [Online]. Available: https://doi.org/10.1016/j.corsci.2010.07.002

Appendix

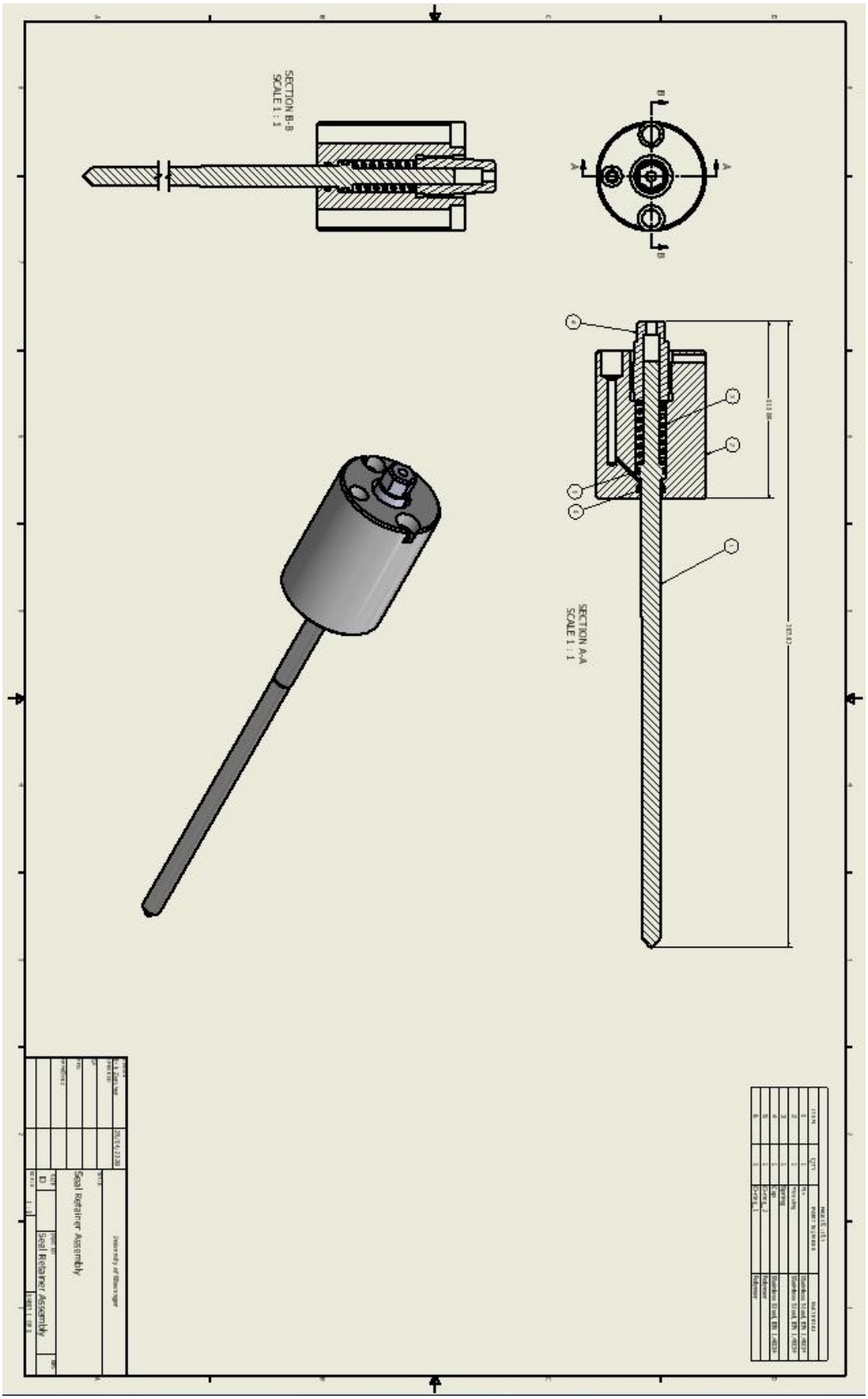
SECTION B-B
SCALE 1 : 1
SECTION A-A
SCALE 1 : 1
Seal Retainer Assembly
Seal Retainer Assembly